Journal of
Synchrotron Radiation
ISSN 1600-5775

Propagation of an X-ray beam modified by a photonic crystal

V. G. Kohn, I. Snigireva and A. Snigirev

J. Synchrotron Rad. (2014). **21**, 729–735

Journal of
Synchrotron Radiation

ISSN 1600-5775

Received 6 March 2014
Accepted 8 May 2014

Propagation of an X-ray beam modified by a photonic crystal

V. G. Kohn,[a]* I. Snigireva[b] and A. Snigirev[b]

[a]National Research Center 'Kurchatov Institute', Kurchatov Square 1, 123182 Moscow, Russia, and [b]ESRF, BP 220, 38043 Grenoble, France. *E-mail: kohnvict@yandex.ru

A method of calculating the transmission of hard X-ray radiation through a perfect and well oriented photonic crystal and the propagation of the X-ray beam modified by a photonic crystal in free space is developed. The method is based on the approximate solution of the paraxial equation at short distances, from which the recurrent formula for X-ray propagation at longer distances is derived. A computer program for numerical simulation of images of photonic crystals at distances just beyond the crystal up to several millimetres was created. Calculations were performed for Ni inverted photonic crystals with the [111] axis of the face-centred-cubic structure for distances up to 0.4 mm with a step size of 4 μm. Since the transverse periods of the X-ray wave modulation are of several hundred nanometres, the intensity distribution of such a wave is changed significantly over the distance of several micrometres. This effect is investigated for the first time.

Keywords: X-rays; photonic crystal; diffraction; imaging; computer simulation.

1. Introduction

Photonic crystals are structures in which the refractive index varies periodically in space on the length scale of the wavelength of light. They possess a photonic band analogue of the electron band gap of semiconductors. High-quality photonic crystals have promising applications in the area of photonics. There are several synthesis methods for preparing photonic crystals. For creating one-dimensional crystals (multilayers) different deposition techniques are used. Two-dimensional crystals can be made by means of the Si microfabrication technique including electron-beam lithography, anisotropic deep plasma etching, LIGA and so on. As for three-dimensional crystals, a widely used technique is the self-assembly of colloid particles on a vertical surface (Klimonsky *et al.*, 2011). The main goal is to realise a situation where all the colloidal particles have the shape of spheres of the same radius, and form a closely packed structure.

When forming a close-packing structure of identical spheres in the first layer, a triangular structure occurs in which the centres of the three neighbouring spheres form an equilateral triangle with the side length equal to the diameter of the sphere, D. Each sphere forms six such triangles with all its neighbours. During the packing of the second layer, spheres lie in the centre of the triangle, but fill only three of the six possible positions. At the formation of the third layer there are two possible combinations. If, in the third layer, spheres occupy the positions as in the first layer, then a hexagonal close-packed (h.c.p.) lattice $ABABAB$ is formed. In the horizontal plane the spheres are ordered with a period D along the selected row and with a period $p = D\cos 30^\circ = 0.866\,D$ perpendicular to this row. Spheres in neighbouring rows are shifted relative to each another by $D/2$. The period in the vertical axis is $h = 2D(2/3)^{1/2}$.

If the third layer is placed over holes in the first and second layers then a face-centred cubic (f.c.c.) lattice $ABCABC$ is created. Thus, the third layer is not equivalent to the first one and all three layers in the structure are different. In such a f.c.c. lattice a horizontal plane corresponds to the direction 111. The period in the vertical axis is $h = 3D(2/3)^{1/2}$.

Both structures are almost equally dense and both are realised in colloidal crystals and often coexist. Colloidal crystals in turn can be used as a template for making inverted photonic crystals with a desired refractive index. In order to obtain crystals with a full photonic band gap the structure needs to be controlled since the photonic band gap is highly sensitive to deformation and defects such as stacking faults, dislocations *etc.* Unfortunately, the method of self-assembly of colloidal particles always creates crystals with a large number of random defects. To achieve perfect crystals, detailed knowledge about the crystal growth mechanism and resulting defect structures is required (Klimonsky *et al.*, 2011).

A major obstacle in studying the defect structure is the lack of appropriate methods that allow the internal structure of a photonic crystal to be seen in three dimensions. The use of transmission electron microscopy in the study of these materials is limited since the techniques' probing depth is a few hundred nanometres. Scanning electron microscopy is restricted to obtaining structural information from the surface. Different optical methods, such as laser diffraction, confocal

optical microscopy and optical spectroscopy, are widely used for the *in situ* characterization of immersed, fluorescent and refractive-index-matched colloidal crystals with particle diameters of the order of a micrometre.

X-ray diffraction is widely used to investigate the crystal structure over macroscopic distances. However, the difficulty of this technique for colloids is the large difference in scale between X-ray wavelength and particle size. To overcome this problem an X-ray high-resolution diffraction scheme based on Fourier transformation by compound refractive lenses was realised (Snigirev *et al.*, 1996; Kohn *et al.*, 2003; Drakopoulos *et al.*, 2005). Such an approach allows the internal structure of the colloidal crystals to be accessed and is indispensable for the study of the internal structure of defects while the structure at the local level remains unsolved (Petukhov *et al.*, 2006; Meijer *et al.*, 2012). X-rays can be used for practically all materials and they do not require index matching or fluorescent labelling. Their shorter wavelength lifts restrictions related to diffraction limitations.

Recently, the high-resolution X-ray microscopy (HRXRM) technique was applied to study mesoscopically structured materials, employing compound refractive lenses (Bosak *et al.*, 2010; Snigireva *et al.*, 2011). The advantage of the lens-based method is the possibility to retrieve a high-resolution diffraction pattern and real-space images in the same experimental set-up. Methodologically the proposed approach is similar to the studies of crystals by high-resolution transmission electron microscopy. The proposed microscope was applied for studying natural and synthetic opals, inverted photonic crystals and colloidal goethite board-like particles (Snigireva & Snigirev, 2013; Meijer *et al.*, 2013; Byelov *et al.*, 2013).

The development of the HRXRM method makes relevant the task of the numerical calculation of the intensity distribution of radiation in the near field, *i.e.* immediately behind the crystal, as well as at short distances. It should be noted that so far such a problem has not been considered. Standard methods of X-ray crystal diffraction are inapplicable, since the photonic crystal has a very long period in comparison with the radiation wavelength. Bragg conditions are fulfilled for a large number of reciprocal lattice vectors, so there is multiple scattering.

Moreover, the scattering from a single sphere cannot be considered weak. The situation is close to the transmission electron microscopy (Cowley, 1995) or channelling effect of fast particles in the crystal (Kagan & Kononets, 1970). On the other hand, the problem can be solved by a method which is used in calculating the X-ray phase contrast (Snigirev *et al.*, 1995). However, this method has to be modified to take into account the strong radiation scattering inside the photonic crystal as well as the strong modulation of radiation in the free space. This paper deals with the development of the method of calculating the transmission of hard X-ray radiation through a thick three-dimensional photonic crystal, and the propagation of a strongly modulated X-ray beam in free space. A computer program has been developed and numerical calculations were performed.

2. Method of computer simulation

X-ray beams delivered at third-generation synchrotron radiation sources have a very small angular divergence; therefore divergence can be neglected in the task of determining the beam transmission in the object or propagation in free space over a small distance. If a parallel beam (a plane wave) propagates through a three-dimensional photonic crystal, a rather pronounced contrast can be obtained only for definite orientations of the crystal. This fact is easy to understand from an analogy with the channeling effect. It is clear that these orientations have to be the ones with the smallest period along the beam direction.

Consider a monochromatic wave of X-ray radiation of frequency ω incident on the entrance surface of a photonic crystal which is normal to the beam direction. The latter coincides with the z-axis of the Cartesian coordinate system (see Fig. 1). The amplitude of the electric field of this wave can be written as follows,

$$E(\mathbf{r}, t) = \exp(ikz - i\omega t)\, A(\mathbf{r}, \omega), \tag{1}$$

where $k = \omega/c = 2\pi/\lambda$ is the wavenumber, λ is the wavelength of monochromatic radiation, c is the speed of light and $\mathbf{r} = (x, y, z)$ is a position in space of the observation point. The function $E(\mathbf{r}, t)$ is a solution of Maxwell's wave equation,

$$\Box E(\mathbf{r}, t) = \frac{1}{c^2}\frac{\partial^2}{\partial t^2}\int \mathrm{d}t'\,\chi(\mathbf{r}, t')E(\mathbf{r}, t - t'), \tag{2}$$

where

$$\Box = \Delta - \frac{1}{c^2}\frac{\partial^2}{\partial t^2}, \qquad \Delta = \frac{\partial^2}{\partial x^2} + \frac{\partial^2}{\partial y^2} + \frac{\partial^2}{\partial z^2} \tag{3}$$

and $\chi(\mathbf{r}, t)$ is the time-dependent susceptibility of matter.

We substitute (1) into (2) and obtain the equation for a slowly varying function $A(\mathbf{r}, \omega)$,

$$\frac{\partial A}{\partial z} = \frac{ik}{2}\,\chi(\mathbf{r}, \omega)A + \frac{i}{2k}\,\Delta A, \tag{4}$$

where $\chi(\mathbf{r}, \omega)$ is a time Fourier image of $\chi(\mathbf{r}, t)$. We note that for X-rays the parameter k has a rather large value, and therefore the second term on the right-hand side of (4) is small compared with the first term even for a relatively small interaction of X-rays with matter which leads to a small value of $\chi(\mathbf{r}, \omega)$. We will assume that the matter is homogeneous, *i.e.* $\chi(\mathbf{r}, \omega) = 2(n - 1)$ is a constant inside the matter, where

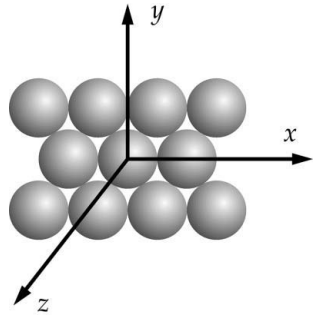

Figure 1
Coordinate axes relative to the photonic crystal.

$n = 1 - \eta$ is a complex refraction index, and $\eta = \delta - i\beta$. However, the matter can be absent in some regions inside the object, and therefore we need to introduce the function $\rho(\mathbf{r})$ which is equal to 1 at a point inside the matter, and 0 at a point in free space.

It is known that for X-rays a paraxial (small-angle) approximation is met with very good accuracy. According to this approximation we can neglect the term $i(2k)^{-1}\partial^2 A/\partial z^2$ which is much smaller than the term $\partial A/\partial z$. Taking into account all assumptions, we finally obtain [see also Kohn (2002) and Kohn (2003)]

$$\frac{\partial A}{\partial z} = -ik\eta\rho(\mathbf{r})A + \frac{i}{2k}\left(\frac{\partial^2 A}{\partial x^2} + \frac{\partial^2 A}{\partial y^2}\right). \tag{5}$$

We have to apply this equation to a photonic crystal where the function $\rho(\mathbf{r})$ changes its value along the z-axis periodically, and the period is rather small. We will assume that we know the function $A(\mathbf{r})$ in the plane (x, y) at some point $z = z_0$ along the optical axis (z). This is the boundary condition for the equation. We want to find a solution in some plane at $z > z_0$.

It is convenient to eliminate the first term on the right-hand side of (5) by means of the substitution

$$A = CB, \qquad C = \exp\left[-ik\eta \int_{z_0}^{z} \mathrm{d}z'\rho(x, y, z')\right]. \tag{6}$$

Then we obtain for the new unknown function B the same boundary condition and the following equation,

$$\frac{\partial B}{\partial z} = \frac{i}{2k}\left[\frac{\partial^2 B}{\partial x^2} + \frac{\partial^2 B}{\partial y^2} + O(\mathbf{r})\right]. \tag{7}$$

Here

$$O(\mathbf{r}) = C^{-1}\left[2\frac{\partial B}{\partial x}\frac{\partial C}{\partial x} + 2\frac{\partial B}{\partial y}\frac{\partial C}{\partial y} + B\left(\frac{\partial^2 C}{\partial x^2} + \frac{\partial^2 C}{\partial y^2}\right)\right]. \tag{8}$$

The term $O(\mathbf{r})$ contains derivatives of C, which is proportional to the integral over the interval from z_0 to z.

The solution of (7) is very complicated. Fortunately, if we consider only a small distance $z - z_0$, then the function $O(\mathbf{r})$ will be small and it can be neglected. Equation (7) without $O(\mathbf{r})$ has the well known solution

$$B(x, y, z) = \int \mathrm{d}x'\,\mathrm{d}y' P_2(\Delta x, \Delta y, \Delta z)B(x', y', z_0), \tag{9}$$

where $\Delta x = x - x'$, $\Delta y = y - y'$, $\Delta z = z - z_0$, $P_2(x, y, z) = P(x, z)P(y, z)$ and

$$P(x, z) = \frac{1}{(i\lambda z)^{1/2}}\exp\left(i\pi\frac{x^2}{\lambda z}\right) \tag{10}$$

is the Fresnel propagator.

Finally, for the initial function we have the solution

$$A(x, y, z) = \exp\left[-ik\eta \int_{z_0}^{z} \mathrm{d}z'\,\rho(x, y, z')\right] \times \int \mathrm{d}x'\mathrm{d}y'\,P_2(\Delta x, \Delta y, \Delta z)A(x', y', z_0). \tag{11}$$

This solution describes two processes. The first process is a transmission through the object layer of small thickness Δz similarly to the free-space propagation. The second process is described by the exponential factor which takes into account the complex phase shift due to the difference of the speed of light in matter compared with in free space, and due to absorption of X-ray radiation in matter. In reality this solution corresponds to the object that is obtained from our object by compressing the layer of thickness Δz to a very thin layer at the position z with the same amount of matter in each point x, y.

It can be shown that within the same approximation the object can be compressed to a thin layer at the position z_0. However, a more accurate approximation corresponds to the situation of a very thin layer with the total amount of matter placed at the middle point of the layer thickness. In this case the X-ray beam propagates through free space over a distance of half the thickness of the layer; then the phase shift is taken into account for the total layer and then the distance of half the thickness of the layer is calculated as in free space once again. Such a solution satisfies the reciprocity principle. We write it in a short form as

$$A(z) = P_2(\Delta z/2) * C\,[P_2(\Delta z/2) * A(z_0)], \tag{12}$$

where the symbol $*$ means a convolution.

In the theory of X-ray phase contrast such an approximation is applied to the total object. Then the factors describing the convolution do not play a significant role; they just add the distance $\Delta z/2$ to the distances before and after the object, and the object can be represented as a zero-thickness plate, but with the correct phase shift according to geometrical optics. The phase factor C alone describes the object. It is called the transmission function.

However, the applicable value for the distance Δz depends on the derivatives of C. In the case of a three-dimensional photonic crystal they are not small. Therefore we cannot apply the solution (12) to the total thickness of the photonic crystal. It is convenient to apply it for one period along the optical axis consisting of two layers in the h.c.p. crystal (structure $ABABAB$), or three layers in the f.c.c. crystal (structure $ABCABC$). In this case the solution (12) should be considered as a recurrent relation which is used iteratively and the factor C is the same on each iteration.

Such an approach is close to the well known 'multi-slice approximation' proposed by Goodman and Moodie [see chapter 11 of Cowley (1995)] for the transmission electron microscopy simulations. We note that X-rays interact with matter quite differently than electrons. For X-rays the main effect is a phase shift of the wavefunction but not an absorption. For a crystal consisting of many periods the free-space propagation over the distance $\Delta z/2$ has to be made only for the first and last periods. In between them, the propagation over the distance Δz can be calculated directly.

Making an analytical estimation of the accuracy of such an approach in the task of calculating the three-dimensional photonic crystal is rather complicated. One can choose a small change of the phase factor $C(x, y)$ for the period as a criterion. It is useful to compare the results of calculations with different values of the step Δz, for example one and two periods.

Another test is a comparison with the experimental data, but first one has to have both theoretical and experimental results.

We note that the X-ray beam, transmitted through the three-dimensional photonic crystal, becomes modulated with a very short period in the plane x, y. In such a case even the task of propagating radiation through free space is rather difficult because a very small step of a numerical set of points is necessary. On the other hand, the total number of points cannot be large. In addition, the intensity of radiation changes significantly over a small distance Δz of propagation in free space, and such modulation is a new physical phenomenon, which has not been observed in experiments so far.

3. Specific example and computing details

For the practical realisation of the method presented above we calculated the transmission of an X-ray beam through a Ni inverted photonic crystal of type *ABCABC* and propagation of a strongly modulated X-ray beam in free space. The considered object was used in the experiment (unpublished). It was prepared by the electrodeposition technique and utilizing a colloidal film as a template. Artificial opals were fabricated using a novel synthetic approach based on electric-field-assisted vertical deposition of monodisperse polystyrene microspheres of average diameter 500 nm onto a Si(100) wafer coated with a 100 nm-thick gold layer.

In order to obtain the free-standing metallic structure on the substrate, the polystyrene microspheres were dissolved by placing the sample in toluene for several hours (Sapoletova *et al.*, 2010). According to scanning electron microscope imaging, the inverse opal consists of nine layers. The X-ray beam is directed along the z axis which is normal to the layers of the photonic crystal (see Fig. 1). The period along the z axis is equal to $h = 3D(2/3)^{1/2} = 1.2247$ μm. The nine layers contain only three periods. The matter thickness for a period is described by the function

$$s(x, y) = \int_{z}^{z+h} \mathrm{d}z'\, \rho(x, y, z') \qquad (13)$$

where z is arbitrary.

Computer simulations are always performed on a finite area on the x, y plane. Since the function $s(x, y)$ is periodical, it is sufficient to perform a calculation inside a region of no more than $2D$. We choose a set of 1024×1024 points with a step of 0.001 μm. Fig. 2 shows the function $s(x, y)$ as a linear black–white contrast in limits of the calculating area. The black colour is used for the minimum value $s_{\min} = 0.1067$ μm and the white colour corresponds to the maximum value $s_{\max} = 0.7331$ μm. The periods of the image are 0.5 μm horizontally and 0.2887 μm vertically.

The computer simulation of the transmission of the X-ray beam through the photonic crystal consists of iterative calculations of the wavefunction $A(x, y)$. We begin with $A(x, y) = 1$. Each iteration includes two operations. The first one is a multiplication of $A(x, y)$ by

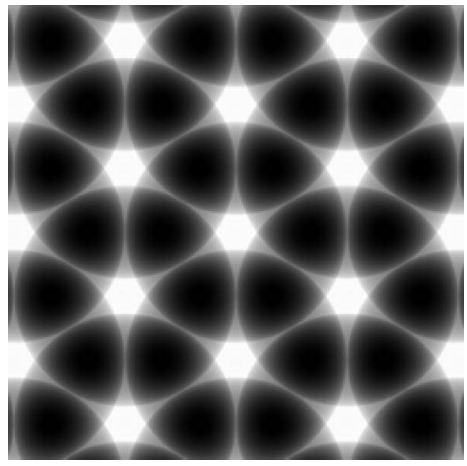

Figure 2
The function $s(x, y)$ within the calculating area. See text for details.

$$C(x, y) = \exp[-ik\eta\, s(x, y)]. \qquad (14)$$

The second operation is a convolution of $A(x, y)$ with the Fresnel propagator $P_2(x, y, h)$. In the last iteration step the propagator $P_2(x, y, h/2)$ should be used. A convolution is performed by means of two Fourier transformations. We calculate the Fourier image of $A(x, y)$, then multiply it by the Fourier image of the Fresnel propagator, which is known in an analytical form, and then calculate the inverse Fourier image of the product. The Fourier image is calculated by means of the fast Fourier transformation (FFT) procedure.

The FFT method computes the result for a finite area, whereas our integrals have infinite limits. Outside the finite area the wavefunction seems to be equal to zero, *i.e.* it is similar to using a slit in front of the object. Therefore the calculation result shows artifacts associated with diffraction by the slit (Kohn & Tsvigun, 2014). Fortunately these artifacts arise only near the boundaries of the calculated area, while the central part is calculated accurately. To eliminate the artifacts we use the property of periodicity for the function $A(x, y)$. Indeed, for an infinite periodical system the accurate result will be periodical at any distance of propagation. Therefore we apply a numerical procedure which selects the central period of $A(x, y)$ and improves the outer area according to the condition of periodicity.

We would like to note that accurate calculation of the X-ray diffraction by a slit shows oscillations with small periods (high frequencies) in the central part of the calculating region as well, but the FFT procedure on the finite number of points washes out these oscillations. This is why the use of a very high number of points is not preferential. On the other hand, in calculating the propagation of X-rays over a small distance we cannot use a large step because the step has to be at least ten times smaller than the first Fresnel zone for a Fresnel propagator, *i.e.* $2(\lambda h)^{1/2}$.

It is necessary to stress that a similar problem exists in calculating the propagation of X-rays in free space. We cannot consider a large distance due to the artifacts arising from a slit diffraction even though the phase shift by matter is absent. We

have to choose the maximum distance for which the artifacts do not influence the central period and perform calculations on this distance iteratively, improving the outer region in each iteration. Therefore the propagation of an X-ray beam over a long distance is impossible with such an approach.

On the other hand, using a small propagation distance iteratively is useful because it allows investigation of a fast transformation of the X-ray beam intensity behind the photonic crystal. This phenomenon has not been studied so far. It shows that the photonic crystal is a perfect modulator of the X-ray beam. The same phenomena exist in electron transmission microscopy.

4. Results and discussion

The elaborated computer program is able to calculate both the transmission of an X-ray coherent wave inside the photonic crystal and the propagation of a strongly modulated wave in free space behind the crystal on the same set of points. At first, the complex wavefield was calculated at the exit surface of the crystal. Since the crystal is thin (only nine layers), the phase shift is the main effect, but not absorption. However, in the points where the Ni thickness is maximal, the absorption of radiation is not small.

The main purpose of our work is calculation of the intensity transformation during propagation in free space behind the crystal. We discover that this transformation is strong even in very small intervals of propagation along the optical axis. The program allows users to save the complex wavefield to a file at each iteration step. These data can be used as a starting point for the next iteration or for creating graphics. In each iteration step the program creates a two-dimensional map of the intensity distribution together with the intensity profiles along the central sections (vertical and horizontal).

The calculations were performed for $\lambda = 0.1$ nm. The distance z along the optical axis is counted from the exit surface of the crystal, and was varied from 0 up to 400 μm with an iteration step of 4 μm; thus we made 100 iteration steps of propagation in free space. Fig. 3 shows four images of two-dimensional intensity maps for distances of 0, 8, 16 and 24 μm. The images are ordered from left to right and from top to bottom. They show only the central part of the calculating area with 512 × 512 points, so they contain just one period horizontally and a longer region vertically to reveal the hexagonal symmetry of the image.

To make the images more informative, the minimum intensity value is shown by the black colour and the maximum value by the white colour, although the contrast is not constant. The dependence of the minimum and maximum relative intensity values on the distance from the crystal (or number of iterations) is shown in Fig. 4. One can see that just behind the photonic crystal the minimum value is 0.67, while in front of the crystal it is 1. The contrast at $z = 0$ is low and has mainly an absorption nature.

With increasing distance z the phase contrast becomes much more pronounced. One can see in Fig. 3 that the intensity distribution deviates more and more from the Ni thickness map, and interference fringes appear in the images. We would like to mention that calculations were performed for the ideal situation, *i.e.* fully coherent radiation and unlimited detector resolution. At present it is impossible to observe these fringes with the experimental HRXRM technique due to the detector resolution (the best resolution is 0.5 μm). In addition, the requirements of the depth of focus of the imaging lens are too severe. A comparison with experimental results will be made in the future.

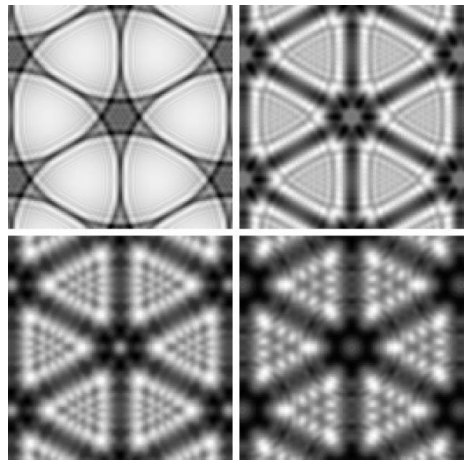

Figure 3
Intensity distributions at distances 0, 8, 16 and 24 μm. The images are ordered from left to right and from top to bottom.

Fig. 5 shows intensity maps calculated for distances z from 40 μm to 400 μm with a step 40 μm, *i.e.* through ten iteration steps. The order of the images is the same as in Fig. 3. We note that in reality the content of the images changes significantly in each iteration step, but it is difficult to show 100 pictures. However, they have some common features. The regions of minimum intensity always correspond to the regions of high Ni thickness.

We note that the strong change of X-ray beam structure over a small distance z is not surprising and can be explained using the Talbot imaging formalism (Talbot, 1836). It is known that the periodical wavefield becomes self-reproduced at the distance $z_T = 2p^2/\lambda$, where p is the transverse period. Indeed, the one-dimensional function $A(x)$ at $z = 0$ can be written as a Fourier series,

$$A(x, 0) = \sum_{m=-\infty}^{\infty} A_m \exp(i2\pi mx/p). \qquad (15)$$

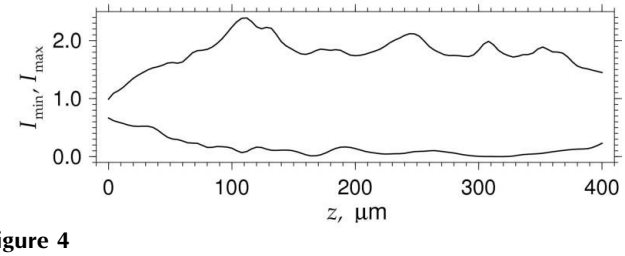

Figure 4
Minimum and maximum values of relative intensity distributions at various distances.

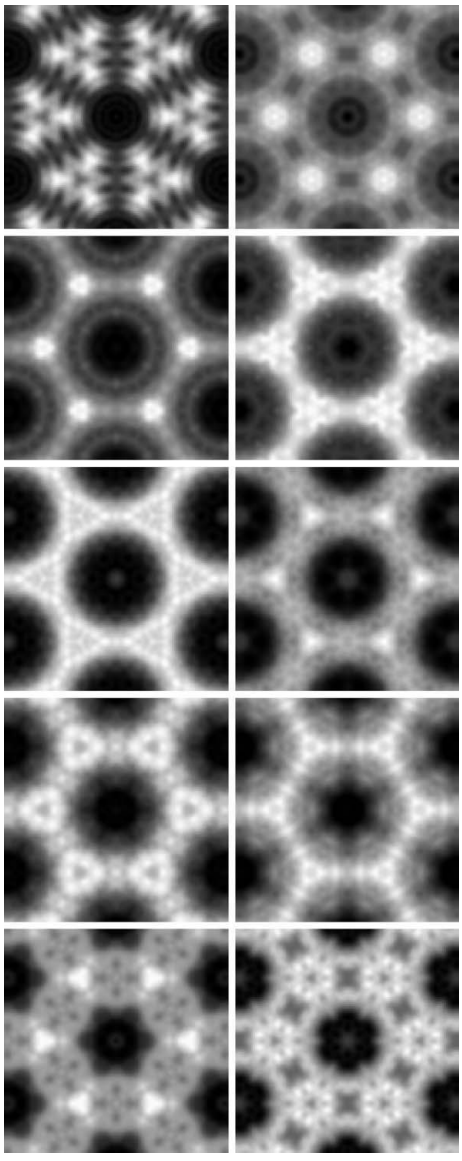

Figure 5
Intensity distributions at distances from 40 μm to 400 μm with a step of 40 μm. The images are ordered from left to right and from top to bottom. See text for details.

Then the convolution

$$A(x, z) = \int \mathrm{d}x' \, P(x - x', z) \, A(x, 0) \qquad (16)$$

has an analytical solution.

The result can be written as follows,

$$A(x, z) = \sum_{m=-\infty}^{\infty} A_m \exp(i2\pi m x / p - i\pi m^2 \lambda z / p^2). \qquad (17)$$

It is easy to see that for $z = z_\mathrm{T}$ the additional phases are a product of 2π and an integer. The crystal under consideration has a vertical period $p = 0.2887$ μm and therefore $z_\mathrm{T} = 1667$ μm. It is four times larger than the calculated maximum distance.

The Talbot effect is similar to the focused image of the object by a refractive lense. In this case a point-to-point correspondence between the wavefields at different places along the optical axis takes place. Another phenomena called the fractional Talbot effect (Berry & Klein, 1996) occurs at distances $z_n = p^2/n\lambda$ which can be very small for large values of n. Our results just demonstrate some fractional Talbot images. They are different from the initial image, and their properties are unknown. Therefore we cannot use the fractional Talbot formalism to verify the calculations.

5. Conclusion

The main result of this work can be formulated as a strong change of the X-ray beam transverse intensity distribution over distances of several micrometres if the wavefield is periodically and strongly modulated. Although the period is half a micrometre or less, the fragments of the distribution are changed on much smaller distances.

This allows one to conclude that the ability of the HRXRM method is not sufficient to observe this effect. It is obvious that the HRXRM method shows a rather smoothed picture due to a finite detector resolution and partial coherence of the X-ray beam.

The methods of calculation of the wavefield inside the photonic crystal as well as in free space behind the photonic crystal are developed on the basis of the FFT procedure and iterational improving the artifacts. The possibility to observe this effect experimentally will be considered in future work.

The work of VGK was partially supported by RFBR grant N.13-02-00469 and by The Ministry of Education and Science of the Russian Federation, project 8364.

References

Berry, M. V. & Klein, S. (1996). *J. Mod. Opt.* **43**, 2139–2164.
Bosak, A., Snigireva, I., Napolskii, K. S. & Snigirev, A. (2010). *Adv. Mater.* **22**, 3256–3259.
Byelov, D. V., Meijer, J.-M., Snigireva, I., Snigirev, A., Rossi, L., van den Pol, E., Kuijk, A., Philipse, A., Imhof, A., Blaaderen, A., van Vroege, G. J. & Petukhov, A. (2013). *RSC Adv.* **3**, 15670–15677.
Cowley, J. M. (1995). *Diffraction Physics*, 3rd ed. Amsterdam: Elsevier.
Drakopoulos, M., Snigirev, A., Snigireva, I. & Schilling, J. (2005). *Appl. Phys. Lett.* **86**, 014102.
Kagan, Yu. & Kononets, Yu. V. (1970). *Sov. Phys. JETP*, **31**, 124–132.
Klimonsky, S. O., Abramova, V. V., Sinitskii, A. S. & Tretyakov, Yu. D. (2011). *Russ. Chem. Rev.* **80**, 1191–1208.
Kohn, V. G. (2002). *JETP Lett.* **76**, 600–603.
Kohn, V. G. (2003). *JETP*, **97**, 204–215.
Kohn, V. G. & Tsvigun, N. V. (2014). *Crystallogr. Rep.* **59**, 1–5.
Kohn, V., Snigireva, I. & Snigirev, A. (2003). *Opt. Commun.* **216**, 247–260.
Meijer, J.-M., Byelov, D. V., Rossi, L., Snigirev, A., Snigireva, I., Philipse, A. & Petukhov, A. V. (2013). *Soft Matter*, **9**, 10729–10738.
Meijer, J. M., Hagemans, F., Rossi, L., Byelov, D. V., Castillo, S. I., Snigirev, A., Snigireva, I., Philipse, A. P. & Petukhov, A. V. (2012). *Langmuir*, **28**, 7631–7638.
Petukhov, A. V., Thijssen, J. H. J., Hart, D. C. 't, Imhof, A., Blaaderen, A. van, Dolbnya, I. P., Snigirev, A., Moussaïd, A. & Snigireva, I. (2006). *J. Appl. Cryst.* **39**, 137–144.
Sapoletova, N., Makarevich, T., Napolskii, K., Mishina, E., Eliseev, A., van Etteger, A., Rasing, T. & Tsirlina, G. (2010). *Phys. Chem. Chem. Phys.* **12**, 15414–15422.

Snigirev, A., Kohn, V., Snigireva, I. & Lengeler, B. (1996). *Nature (London)*, **384**, 49–51.
Snigirev, A., Snigireva, I., Kohn, V., Kuznetsov, S. & Schelokov, I. (1995). *Rev. Sci. Instrum.* **66**, 5486–5492.
Snigireva, I., Bosak, A. & Snigirev, A. (2011). *AIP Conf. Proc.* **1365**, 289–292.
Snigireva, I. & Snigirev, A. (2013). *J. Phys. Conf. Ser.* **463**, 012044.
Talbot, H. F. (1836). *Philos. Mag.* **9**, 401.